A seismic sequence from Northern Apennines (Italy) provides new insight on the role of fluids in the active tectonics of accretionary wedges

Giovanna Calderoni, Rita Di Giovambattista, Pierfrancesco Burrato, Guido Ventura

Istituto Nazionale di Geofisica e Vulcanologia, Via di Vigna Murata 605 - 00143 Roma, Italy;

Corresponding author: G. Ventura, Istituto Nazionale di Geofisica e Vulcanologia, Via di Vigna Murata 605 - 00143 Roma, Italy; Phone +39 06 51860221 – e-mail: ventura@ingv.it

Abstract

We analyze a seismic sequence which occurred in 2000 along the Northern Apennines accretionary wedge (Italy). The sequence developed within the Cretaceous-Triassic limestones of the tectonic wedge, where methane-rich and oil reservoirs are stored. Ruptures mainly developed on WNW-ESE striking thrusts. The compressive stress field is consistent with that acting at regional scale in Northern Apennines. Seismic parameters indicate that fluids are involved in the seismogenic process. The amplitudes of the P and S phases and data from some stations evidence a P to S conversion within Vp/Vs=2.1 layer. The attenuation properties of crust show a higher attenuation zone located west of the epicentral cloud. Eight hundred aftershocks delineate a sub-vertical cloud of events between 7 and 14 km depth. The space-time evolution of the aftershocks is consistent with a diffusive spreading (diffusivity=1.9 m^2/s) along vertically superimposed thrusts. Diffusion also controls the time evolution of the sequence. Fluid pressure is estimated to be roughly equal to the vertical, lithostatic stress. The overpressure within reservoirs develops by tectonic compaction processes. The fluids upraise along sub-vertical fractures related to the shortening of the wedge. The 2000 sequence occurred in an area that separates a thermal and deeper petroleum system from a shallower biogenic system. The divider of these systems controls the attenuation properties of the crust. The fluid-rock interaction at seismogenetic depth is related to hydrothermal processes more than to compaction. In accretionary wedges, seismicity activating superimposed thrusts may drive methane and oil upraising from the upper crust.

Key-words: Seismicity, fluids, accretionary wedge, thrust, geodynamics, Northern Apennines

1. Introduction

Studies of geochemistry and on vein structures, as well as data from boreholes and seismic lines evidence that fluids play an important role in the evolution of accretionary wedges (e.g. Karig et al., 1973; Cochrane et al., 1994; Bangs et al., 1999; Labaume et al., 2001; Brown et al., 2003; Yonkee et al., 2003; Perez et al., 2004; Kondo et al., 2005). High fluid pressures facilitate the decoupling and activation of low-angle thrusts and formation of pop-up structures (Mourgues and Cobbold, 2006). It is shown that fluid flow, variation of pore fluid pressure, and deformation in thrust zones can trigger seismicity (Gratier, 2002; Sibson, 2005), although the relationship among thrust tectonics, fluids and seismicity is poorly understood compared to strike-slip regimes like the San Andreas Fault (Malin et al., 2006), extensional regimes like central Italy and Corinthe (Greece) (Miller, 1996; Moretti et al., 2002; Antonioli et al., 2005).

On 8 May 2000 at 12:29 (UTC), a moderate-size (M_D = 4.3) earthquake followed by aftershocks occurred close to the outcropping thrust front of the Northern Apennines accretionary wedge (Italy), in an area characterized by mud-volcanoes, fluid venting, oil and gas reservoirs (Fig. 1a; Picotti et al., 2007; Picotti and Pazzaglia, 2008). As such, the study of this sequence provides a unique chance for (1) the analysis of the seismogenic processes occurring in thrust zones and (2) the effects of fluids on the physical parameters of the accretionary wedges. Here, we analyse the seismicity in light of the available information on the tectonic and structural pattern. The spatial-temporal evolution of the sequence, i.e. the diffusivity, is investigated and a variety of seismic attributes such as velocity and attenuation are evaluated. We highlight the role played by thermal fluids in the evolution of the sequence, estimate the fluid pressure at seismogenetic depth, and evidence how the study of seismic sequences in thrust zones can be used to characterize oil reservoirs. A comparison between the reservoirs of strike-slip zones and those occurring in thrust areas is presented. The collected data provide new insights on the relationships between fluids and active accretion processes. The seismotectogenesis of the Apennine wedge and its geodynamic implications are also discussed.

2. Geological framework

A seismic sequence started on 8 May 2000 in the area of Faenza city, which is located close to the external topographic margin of the Northern Apennines (NA) fold-and-thrust belt (Fig. 1a). NA is a Neogene-Quaternary, NE-verging belt developed in the framework of the European-African convergence and involved the westward subduction of the Adriatic lithosphere (Alvarez, 1972; Doglioni, 1991). During the convergence, the roll-back of the W-subducting Adriatic slab induced the eastward migration of the thrust fronts and foredeep basins. The youngest of these basins is the Po Plain. The structural setting of NA and its evolution were reconstructed using deep seismic reflection data (CROP03 line; Barchi et al., 1998), which recognized the thick-skinned geometry of the thrust system (Lavecchia et al., 2003 and references therein).

The NA physiographic margin is represented by the Pedeapenninic Thrust Front (PTF; Boccaletti et al., 1985). PTF consists of a system of faults that separates the uplifted and exposed accretionary wedge from the Po Plain. In the Po Plain, the more external NA thrust fronts are buried beneath a thick sequence of Plio-Quaternary sediments (Fig. 1a,b; Doglioni, 1993; Bartolini et al., 1996; Picotti, and Pazzaglia, 2008). The NA thrust fronts migrated at about 9 mm/yr and the present-day activity concentrates on PTF and the outer fronts (Basili and Barba, 2007). The structural configuration of the external NA fronts was mapped using subsurface geological data derived from commercial seismic reflection lines and borehole data (e.g.: Pieri and Groppi, 1981; Massoli et al. 2006). The NA tectonic elements follows three main arcs (Fig. 1a): Monferrato, Emilia and Ferrara-Romagna arcs. The Ferrara-Romagna arc is further subdivided into three relatively minor structures: the Ferrara, Romagna and Adriatic folds. The southern Po Plain is a flat, low relief region, and the only expression of the active buried anticlines is their control on the drainage pattern (Burrato et al., 2003). Tectonic activity of the NA thrust fronts is testified by (a) historical and instrumental seismicity (CPTI, 2004; CSTI 1.0, 2001; Castello et al., 2005), the latter characterized by reverse focal solutions (Pondrelli et al., 2006), (b) surface geological and geomorphological evidence of faulting and folding of recent deposits (Vannoli et al., 2004;

87 Boccaletti et al., 2004), and (c) subsurface geophysical profiles showing very recent growth strata
88 developed across buried anticlines (e.g.: Scrocca et al., 2007). Borehole breakouts and focal
89 mechanisms of crustal earthquakes show a maximum horizontal stress axis oriented perpendicular
90 to the strike of the thrust front (Montone et al. 2004).

91 The epicentral area of the 2000 Faenza seismic sequence is structurally located between PTF
92 and the inner Romagna folds. In this sector of the Po Plain, the thickness of the base of the Pliocene
93 reaches more than 5000 m, while it is less than 1000 m on top of the anticlines (Fig. 1b). Numerous
94 historical earthquakes are registered in the catalog. The strongest earthquakes occurred in 1688 (M_w
95 5.9, Romagna earthquake) and in 1781 (M_w 5.8, Faentino earthquake) (CPTI, 2004). The Italian
96 Database of seismogenic sources reports that the causative faults of the two largest historical events
97 were two N-verging blind thrusts belonging to PTF and to the outer Romagna folds (DISS Working
98 Group, 2007; Basili et al., 2008). Active compression across the Po Plain is testified by the S-
99 verging seismogenic structures belonging to Southern Alps chain (SA in Figure 1a), which follows
100 the margin of the plain in the Veneto-Friuli area (Burrato et al., 2008). On the other hand, aside of
101 the 2000 Faenza sequence, few and sparse instrumental seismicity is recorded. Like the other
102 moderate events of the area (Di Giovambattista and Tyupkin 1999), the 2000 sequence was
103 preceded by activation of weak earthquakes.

104 The NA external sector is characterized by numerous active seeps of deep fluids that include
105 mud volcanoes and methane vents (Fig. 1a,b; Bonini, 2007; Etiope et al., 2007). The geochemical
106 analyses of the gas, which reaches an output rate of 6 t d^{-1}, indicate a thermogenic source deeper
107 than 6 km. This source is within the Cretaceous limestones found below the Miocene foredeep
108 deposits (Capozzi and Picotti, 2002). The presence of the seeps highlight the occurrence of buried
109 and outcropping active reverse faults and related anticlines (Martinelli and Judd, 2004; Bonini,
110 2007). The hydrocarbon generation and migration domain is hosted and trapped by the buried
111 thrusts and anticlines of the NA chain. The Miocene reservoirs located in the Ferrara folds are
112 charged by gas/liquids likely derived from a Triassic source, thus accounting for a Miocene-Triassic

113 petroleum system (Fig. 1a inset) (Lindquist, 1999). On the contrary, the reservoirs within the
114 Romagna-Adriatic folds and in the central Po plain are charged by biogenic to mixed thermogenic
115 gas. These latter occur at shallower depths and are stored within the upper Miocene-Pliocene
116 deposits (Fig. 1b). The marine to continental Plio-Quaternary sedimentary sequence hosts three
117 regional groups of fresh water aquifers (RER, ENI-Agip, 1998). In the epicentral area of the 2000
118 earthquake, these aquifers reach a maximum depth of about 700 m below the sea level (Fig. 1b,c).
119 The aquifers are separated by regionally continuous impermeable layers. They are fed by meteoric
120 infiltrations into gravel and sand bodies (Fig. 1b,c) that form the alluvial fans at the mountain front
121 and fill the main alluvial valleys. Brines are confined within the Miocene hydrocarbon seeps at a
122 maximum depth of 5-6 km (Fig. 1b,c; Picotti et al., 2007).
123
124 **3. The 2000 Faenza seismic sequence**
125
126 *3.1 Data*
127
128 A temporary seismic network composed of 8 stations was installed by the Istituto Nazionale
129 di Geofisica e Vulcanologia (Italy) after the mainshock (M_D=4.3) occurred on 8 May 2000 at 12.29
130 UTC. All stations (blue triangles in Fig. 1) have 3 components of seismographs (Reftek CMG45T,
131 Lennartz LE 3d-5s) and a sampling rate of 100 Hz. The observations lasted for about a month and
132 more than 800 aftershocks were detected. P- and S-wave onsets were hand picked on digital
133 waveforms obtaining an accurate timing.
134
135 *3.2 Waveforms analysis*
136
137 Waveforms are examined for 20 events with $M_D \geq$ 3.0. The analysis of the seismograms
138 shows a prominent difference in the first P-waves recorded among the stations CAST and COLL
139 and the other ones (Figs. 1 and 2). CAST and COLL waveforms have a high content of high

frequency, whereas the other stations show a high attenuation to low frequencies (Fig. 2). The first arrivals at all the stations, excluding CAST and COLL, have an onset with a sharp impulse on the vertical component and a very low amplitude onset on the horizontal components. On the contrary, the S phase is strongly amplified in the horizontal components and is lacking in the vertical components. This feature suggests different attenuation properties of the medium, possibly related to the azimuthal distribution of the stations with respect to the hypocenters. The analysis of the seismograms shows a strong P-to-S converted phase (Ps) with larger amplitude arrives about 1 s after the first P arrival at the stations TULL, FILE and CESA (Fig. 2). It is worth noting that the converted phase is not systematically observed at the same stations for all the events. The Ps phase is not observed at stations CAST and COLL, which are at less then 15 km from the station TULL. We roughly estimated the depth at which the Ps conversions occur using the velocity values obtained as reported in following section. For a P-wave with a vertical incidence converted to an S-wave at a depth z, $z=\Delta t V_P V_S/(V_P-V_S)$ with Δt the time between the arrival of the direct P-wave and the converted Ps phase. In the nearest stations, the angle of incidence is almost vertical and the above relation gives a reliable estimate of z. For the analysis of the converted waves, we considered the stations TULL and FILE, which show the strongest amplitude of the Ps phase. The estimated z is of about 6 km for FILE and 3 km for TULL. This result indicates that the Ps phase was caused by the conversion of a scattering zone that, in light of the available geological data, corresponds to Quaternary sediments (see Fig. 1).

3.3 Velocity structure and event location

A realistic velocity model is obtained by inverting the arrival times of the selected 592 earthquakes with a minimum of 12 observations, root mean square (rms) $\leq$1 s, and azimuthal gap $\leq$160°, by applying the VELEST inversion code (Kissling et al., 1995). The velocity model consists of parallel, laterally homogeneous layers whose thicknesses are not perturbed during the inversion. After performing several tests with different initial velocity models, we observed that a single minimum 1-D model with three layers is well resolved. A wide range of starting velocity models

with more layers have been tested but the data do not support complicated starting models, probably due to significant lateral heterogeneity. Figure 3a shows the a priori and the calculated velocity model. The computed minimum 1-D model shows V_P/V_S=2.1 at depth ≤ 8 km. This anomalous value of V_P/V_S could be due to the presence of fluids, as already reported for other areas worldwide (e.g., Eberhart-Phillips and Michael, 1993; Zhao et al., 1998; Husen and Kissling, 2001). The obtained high V_P/V_S is also confirmed by the modified Wadati diagram obtained with a subset of clearly recorded P and S arrivals (Fig. 3b), which have weight equal to 0 and 2, respectively. Results from the Wadati diagram shows V_P/V_S =2.324±0.08.

The crustal model of Fig. 3a is used to relocate the aftershocks by means of the HYPOELLIPSE code (Lahr, 1999), resulting in a significant improvement in the quality of hypocentral parameters (rms <0.10 s). The relocated events show two main alignments of epicentres (Fig. 4a, b). The main alignment is elongated in the direction of the thrust belt, which is WNW-ESE. The other alignment is located at the northwestern tip of the main one and roughly strike NE-SW. In a NE-SW section, the hypocenters fall on a vertical cloud at depths between 7 and 14 km (Fig. 4c). Earthquakes of the main, NW-SE alignment are located at depth between 7 and 12 km, whereas the events of the NE-SW alignment occur at depth between 7 and 14 km (Fig. 4b). The spatial-temporal evolution of the aftershocks describes an outward spreading. In particular, the early seismicity developed in the central-western sector of the NW-SE alignment while the successive events migrate towards the tips of the aftershock cloud (Fig. 4a). Therefore, the previously described vertical cloud of events developed in a later time.

3.4 Seismic attenuation

Previous studies have shown that a high V_P/V_S value correlates with high P-wave attenuation (Tompkins and Christen, 1999) as well as with increased S-wave attenuation (Winkler and Nur, 1982). Having found a high V_P/V_S in our study area, we estimate the seismic attenuation of the source area. We followed the common procedure of the Standard Spectral Ratio method (SSR),

196 which consists in determining the site amplification at each station with respect to a reference site.
197 To select the reference site, we examined the ray path followed by seismic rays from the
198 hypocenters of earthquakes with $M_L \geq 3.8$. The seismic rays of the selected events travel to the
199 reference station CAST without crossing the Quaternary attenuative zone (see section 2). On the
200 contrary, the seismic rays travelling to the other seismic stations cross the attenuative zone.
201 Although most attenuation mechanisms indicate some frequency dependence, mainly for
202 frequencies ≥100 Hz, most measurements of Q with body waves are obtained using a constant Q_S
203 model (Flanagan and Wiens, 1994). In this study, we select a frequency range of 2-10 Hz. If the
204 source spectra obey the ω^2 approximation with constant stress drop (Boore, 1983), the acceleration
205 spectrum $A_o(f)$ radiated from a point-source in the far-field approximation is:
206
207 $$A_o(f) = \frac{F_S R_{,\varphi} P}{4\pi\rho\beta^3} \frac{M_0}{1+(f/f_0)^2} (2\pi f)^2 G(R) \exp\left(-\frac{\pi R f}{\beta Q_S}\right) \quad (1)$$
208
209 To estimate $A_o(f)$, we used a 3s time window beginning 0.5s before the body wave by applying a
210 10% cosine taper to remove the scattering effects. In equation 1, F_S is a free-surface coefficient (2),
211 $R_{\vartheta,\varphi}$ is the RMS value of the radiation pattern (0.63), P is the horizontal composition factor ($2^{1/2}$),
212 and ρ is the density (2700 kg/m^3). Shear-wave velocity β in the crust is taken as 3.2 km/s. M_0 and f_0
213 are the seismic moment and the corner frequency, respectively. The values of M_0 were taken from
214 the MedNet web site (http://www.ingv.it/seismoglo/RCMT/); the corner frequencies were computed
215 following Brune (1970). $G(R)$ is the geometrical spreading deduced by Malagnini et al. (2000):

216 $$f_o = \frac{4.9 \cdot 10^6 \beta \Delta\sigma^{1/3}}{M_0^{1/3}} \quad (2)$$

217 $$G(R) = \begin{cases} R^{-0.9} & R < 30 \text{ km} \\ R^{0} & 30 < R < 80 \text{ km} \\ R^{-0.5} & R > 80 \text{ km} \end{cases} \quad (3)$$
218
219
220
221 where R is the hypocentral distance. The exponential term in equation (1) represents the empirical
222 attenuation function used to compensate the spectral attenuation along the propagation path. We
223 selected 20 seismic events with $M_L > 2.0$. Hypothesizing a different attenuation among CAST and

224 the other stations, we computed $Q_{S,Staz}$ as the mean value of the attenuation calculated at each
225 station and corresponding to the fixed values of $Q_{S,CAST}$ (Table 1). The mean $Q_{S,Staz}$ values are
226 obtained discharging data exceeding 2 standard deviation from the mean value. As shown in Fig. 5,
227 the stations are characterized by two different attenuation values that separate the rupture zone in
228 two sectors. Stations CESA, FILE, TOME and TULL show significantly higher attenuation values
229 with respect to COLL, SGIO and PETE (Table 1). Therefore, the 2000 sequence occurred between
230 two zones with different attenuation properties. The ratio of the attenuation of the two zones is
231 about the same with respect to the value of the attenuation assumed for the reference station. A
232 $Q_{S,CAST}$ value of 100, in combination with the other values of $Q_{S,Staz}$ and with the ω^2 model
233 (equation 1) provides the best fit of the spectra (Fig. 6). In any case, the low *Qs* values (Table 1)
234 show that the zone covering the Quaternary basement is strongly attenuative even if this feature
235 does not justify the occurrence of two zones laterally characterized by a significant differences in
236 *Qs*. An interpretation of this feature is discussed in the section 4.

237
238 *3.5 Focal Mechanisms*

239
240 We computed focal mechanism by means of the standard fault plane fit FPFIT grid-search
241 algorithm (Reasenberg and Oppenheimer, 1985). We obtained well-constrained focal mechanisms
242 for 154 events with more than 7 polarities, maximum azimuthal gap of 180° and hypocentral error
243 less than 1 km (Fig. 7a). The average errors on the maximum likelihood solutions are ≤10° for
244 strike, dip and rake. The distribution of the sub-horizontal P-axes shows a NNW-SSE preferred
245 strike, whereas the T-axes are sub-vertical. Nodal planes of focal mechanisms show a clear WNW-
246 ESE preferred strike (Fig. 7b). This strike is consistent with the WNW-ESE elongation of the 2000
247 aftershock zone (Fig. 4a). The dip of nodal planes concentrates between 45° and 65° and the rake
248 values indicate prevailing thrust- to oblique-type ruptures (Fig. 7b). These ruptures are consistent
249 with those of the 2000 mainshocks, which also show thrust-type faulting (Fig. 1). Second-order
250 strike-slip faulting (rake~0°) along NW-SE to N-S striking planes also occur. Temporal evolution
251 from thrust to strike-slip faulting, or the opposite, have been not observed. We use the computed

252 focal mechanism to determine the stress field using the method developed by Gephart and Forsyth
253 (1984). Results are reported in Fig. 7c and indicate a reverse stress field characterized by a
254 subhorizontal, NE-SW striking maximum compressive stress σ_1 and a vertical minimum
255 compressive stress σ_3. The value of $R=(\sigma_1-\sigma_2)/(\sigma_1-\sigma_3)$ is 0.2. This low value implies that σ_1
256 approaches σ_2, so suggesting a possible switch between σ_1 and σ_2. This switch explains the
257 coexistence, within the same stress field, of thrust and strike-slip ruptures.

258
259 **4. Discussion**
260
261
262 *4.1 Structural significance of the 2000 seismicity*
263
264 The data presented here show that the Northern Apennines 2000 sequence developed along a
265 WNW-ESE striking rupture zone, which mainly extends from 7 to 16 km depth. Second-order
266 ruptures roughly aligned NE-SW occur at the northwestern tip of the main WNW-ESE zone. The
267 preferred strike of nodal planes indicates WNW-ESE faulting and the stress field from focal
268 mechanisms suggests compression along a subhorizontal NE-SW striking axis. This stress
269 configuration is that acting in Northern Apennines and it is characterized by a compressive stress
270 field with σ_1 orthogonal to the chain axis. (Montone et al., 2004). The kinematic picture resulting
271 from the 2000 sequence indicates thrust-type faulting along planes located at different depth. In this
272 frame, the (few) strike-slip focal mechanisms, which suggest left-lateral movements along NE-SW
273 faults, concentrated on the NE-SW second-order, tip structure. These second-order ruptures can be
274 interpreted as lateral ramps of the main thrusts. Our data indicate that the Faenza sequence
275 developed below the Pedeapenninic Thrust Front, which represents the accretionary wedge of the
276 chain, and, in particular, of the Ferrara-Romagna arc (Fig. 1). In this area, the base of the Pliocene
277 units is at about 5 km depth, whereas at the top of the Po Plain anticlines, the Pliocence thickness is
278 less than 1 km (Fig. 1a,b; Pieri and Groppi, 1981). Therefore, the 2000 seismicity did not affect the
279 Plio-Quaternary successions. Taking into account this observation and the subvertical elongation of
280 the seismic cloud, we suggest that the ruptures developed along a subvertical fracture zone that

281 crosses overlapping, buried thrust surfaces whose fronts are located within the Po plain. The
282 occurrence of this fracture zone is consistent with the structural features of thrusts zones like the
283 Wheeler Ridge oil field in California, where sub-horizontal micro-fractures and veins parallel to the
284 thrust front coexist with vertical fracture networks (Perez et al., 2004).
285
286 *4.2 Evidence of fluids*
287
288 The area affected by the 2000 earthquakes is characterized by mud volcanoes and methane
289 vents (Fig. 1; Bonini, 2007). In addition, oil and methane reservoirs occur generally at depths
290 between 5 and 10 km, within the Cretaceous-Triassic limestones underlying the Miocene foredeep
291 deposits (Lindquist, 1999; Capozzi and Picotti, 2002; Etiope et al., 2007). As a result, the focus of
292 the 2000 seismicity mainly concentrates within a sector of the upper crust in which thermogenic
293 methane and oil reservoirs occur. Therefore, these deep fluids could play a role in the seismic
294 release. This hypothesis is supported by our results, which can be summarized as follows:
295 (a) The overall Vp/Vs is 2.32. This value is anomalously high for the Northern Apennines
296 (Vp/Vs~1.8-1.9; Piccinini et al., 2006; Ciaccio and Chiarabba, 2002) and it is consistent with values
297 estimated in fluid-rich zones (Zhao and Negishi, 1998; Husen and Kissling, 2001).
298 (b) The occurrence of a P to S conversion mainly recorded at the stations FILE and TULL.
299 The converted phase arrives about 1 s after the first P arrival. This conversion could mark an
300 impedance contrast interface possibly related to the occurrence of a fluid-rich zone(s) at depth
301 larger than 3 km (TULL station) and 6 km (FILE station), lacking structural or geophysical
302 evidence of a lithological/structural discontinuity able to explain the observed impedance contrast.
303 Even if our data cannot unequivocally locate the interface of the conversion, this occurs at the
304 transition between the Cretaceous-Triassic limestones, which are the host rocks of the oil and
305 methane reservoirs, and the uppermost Pliocene deposits, which constitute an efficient permeability
306 barrier.

(c) in a transversal section, the 2000 hypocenters delineate a sub-vertical conduit-like cloud. (Fig. 1). We remark that this vertical distribution of hypocenters has not been previously observed in the Northern Apennine sequences, which are generally characterized by distributions consistent with low angle (<45°) surfaces (Ciaccio and Chiarabba, 2002; Piccinini et al., 2006). The geometric features and outward spreading of the 2000 Faenza aftershocks is typical of pore-pressure perturbation processes (Audigane et al., 2002; Shapiro et al., 1997; 2003). To test the hypothesis that the 2000 sequence could be related to these processes, we analyze the spatial-temporal distribution of seismicity following Shapiro et al. (2003).

4.3 Pore-pressure diffusion and triggering mechanism

A number of diffusion-typical signatures have been documented in the spatio-temporal distribution of seismic clouds (see Shapiro et al., 1997; 2003). In an effective isotropic, homogeneous poroelastic medium, the extension of the rupture zone can be approximated by a theoretical curve $r=(4\pi Dt)^{1/2}$ that describes the distance r of the pressure front from the fluid source (triggering front) as a function of the diffusivity D and time t (Shapiro et al. 1997). The parabolic fitting of a cloud of events provides the effective scalar estimates of D. In Fig. 8, a spatio-temporal distribution of the relocated 2000 Faenza seismicity of the second pattern is shown. A good agreement between the theoretical curve with D=1.9 m^2/s and the data can be observed: the events concentrate within the parabolic envelope as theoretically expected for diffusive, pore-pressure related seismic processes. The obtained D value is within the range (0.02-9.65 m^2/s) of those estimated for pore pressure diffusion processes in the upper crust (Talwani et al., 2007 and references therein).

334 *4.4 Estimate of the fluid pressure*

335

336 Here, we present an estimate of the fluid pressure acting at depth during the 2000 sequence.
337 We follow the approach of Fournier (1996), as modified by Ventura and Vilardo (1999). According
338 to Fournier (1996), we assume a Coulomb criterion of failure using the following analytical
339 expression for rupture along a plane:

340

341 $$(\sigma_1-\sigma_3) = [2\mu(\sigma_3-\lambda\sigma_V) + 2C]/[(1 - \mu\tan\theta)\sin 2\theta] \quad (4)$$

342

343 where μ is the coefficient of internal friction, C is the cohesion, θ is the angle between the
344 maximum principal stress σ_1 and the fault plain, and λ is the ratio between the fluid pressure Pf and
345 the vertical stress σ_V which, in a compressive stress regime, is $\sigma_3 = \rho gh$, where ρ is the rock density,
346 g is the acceleration of gravity, h is the thickness of overburden. For the 2000 sequence, we assume
347 that faulting occurs on pre-existing planes of weakness and set C=0. This assumption is justified by
348 the observation that the thrust-type events affect a zone where several juxtaposed thrusts occurs
349 (Massoli et al., 2006). According to Byerlee (1978), μ is generally between 0.6 and 0.75. Here, we
350 select 0.6. Assuming ρ=2700 kg/m^3, the value of σ_3 at 10 km of depth, which represents an average
351 depth of the hypocenters, is ~250 MPa. According to data from a well located 15 km west of the
352 epicentral cloud, σ_1 varies with depth at 35 MPa/km (Mariucci and Muller, 2003). Therefore, at 10
353 km of depth, σ_1=350 MPa. On the basis of the results from the inversion of focal mechanisms (Fig.
354 7c), θ is assumed to be 45°. We resolve equation 4 with respect to Pf and found λ=0.86, i.e. Pf =
355 215 MPa at 10 km of depth. This value of λ suggests a high fluid pressure with $Pf \sim \sigma_3$, and nearly
356 lithostatic stress conditions. According to Sibson (2000), lithostatically pressured fluids were
357 trapped in the crust by the compressive stress field, and episodically released through a fault-valve
358 mechanism. This agrees with the general structural features of the area where the 2000 sequence

359 occurred, which is characterized by episodic release of methane-rich fluids from reservoirs located
360 within the 5-10 km deep Triassic-Cretaceous reservoirs. In addition, our result supports the
361 theoretical model by Orlov et al. (2004) on the incidence of tectonic stress on overpressure.
362 According to this model, a variation of tectonic stress in folded areas may induce an overpressure in
363 fluid reservoirs that are in lithostatic equilibrium. In the area of the 2000 seismic sequence, the
364 value of the fluid pressure is roughly equal to the minimum compressive stress. This suggests that
365 the main factor controlling the overpressure in the hydrocarbon domain of Apennines is the
366 horizontal shortening of the chain, i.e. tectonic compaction. We exclude the involvement of other
367 processes, e.g. elevation of the hydraulic head (Schneider, 2003) or loading of the overburden
368 (Roure et al., 2005), because the 2000 seismicity develops at a depth of 7 to 14 km, where the effect
369 of the overburden or hydraulic head are practically null.
370
371 *4.5 Seismic attenuation vs. spatial distribution of reservoirs*
372
373 The observed larger attenuation at the seismic stations CESA, FILE, TOME, and TULL,
374 which are located northwest of the 2000 seismic cloud, with respect to that at CAST, COLL, SGIO,
375 and PETE, located to the southeast, is not due to the different thickness of the Plio-Quaternary
376 sediments because the attenuation among the seismic stations appears not related to the thickness of
377 sediments. The attenuation path could be explained taking into account the different depth and
378 origin of oil reservoirs in this sector of the Northern Apennines. In particular, the reservoirs located
379 northwest of the 2000 cloud mainly occur at depths comparable with the hypocenters of
380 earthquakes. These carbonate reservoirs are locally charged by gas and liquids derived from
381 Triassic sources (Fig. 1a,b; Lindquist, 1999). On the contrary, the carbonate reservoirs to the
382 southeast of the epicentral cloud are charged by biogenic to mixed biogenic-thermogenic gas and
383 occur at shallower depths, being stored within the upper Miocene-Pliocene siliciclastic deposits.
384 Therefore, at hypocentral depths, which concentrate below 7 km, the observed larger attenuation at

385 the stations CESA, FILE, TOME, and TULL could reflect the higher fluid content of the host rocks
386 due to the occurrence of the northwestern and deeper reservoirs. We exclude that surface/subsurface
387 waters (e.g., shallow acquifers, rain fall, lakes; Muco, 1998) play a role in the triggering mechanism
388 of the 2000 sequence because of (a) the hypocentral cloud does not affect the upper 7 km of the
389 crust, (b) the maximum depth of the aquifers is 700 m, and (c) the lack of seasonality, i.e.
390 periodicity, in the temporal evolution of the sequence.
391
392 *4.6 Geodynamic implications*
393
394 Our results and previous studies (Picotti et al., 2007 and references therein) clearly indicate
395 that accretion processes are still currently active in the Northern Apennine and operates within a
396 well known petroleum province, as attested by the presence of oil wells and gas seepages degassing
397 along the northern arc of Apennines. Fluids may be involved in other seismic sequences and may
398 play a major role in the development of thrusts. From a geodynamic point of view, it is worth
399 nothing that while the seismicity related to the extensional strain field affecting the inner sectors of
400 the Apennine chain is mainly due to the uprising of CO_2 fluids from the mantle ($\delta^{13}C$ in CO_2
401 between -4 and -8 and $0.2<{}^3He/{}^4He$ (R/Ra)<2.4; Minissale et al., 2000; Chiodini et al., 2004), our
402 results indicate that the earthquakes related to the compression acting in the outer sectors of the
403 chain and in the Po Basin involve methane-rich fluids upraising within the upper crust (Etiope et
404 al., 2007), lacking evidence of significant CO_2 degassing. The few CO_2 released along the chain
405 axis has $\delta^{13}C>-4$ and ${}^3He/{}^4He$ (R/Ra) <0.4, thus suggesting an organic (biodegradation) to
406 thermogenic (<300°C) origin (Minissale et al., 2000). According to Picotti et al. (2007), the
407 reservoirs drilled in the Po Plain are located within the Miocene sequences at a maximum depth of
408 5-6 km; the hydrocarbons of these traps have a relatively low thermal maturity. The occurrence of
409 deeper reservoirs located in the Mesozoic and Triassic sequence at a depth between 5-6 and 10 km
410 is documented by the thermogenic imprint of the methane (see lithostratigraphic column in Fig.

411 1c). In light of these geological data, our data suggest that the tectonic stress induced an
412 overpressure in the 5-10 km deep reservoirs and a fluid migration towards the shallower ones.

413 The geochemical features of Northern Apennines-Po Basin petroleum system, which is
414 associated with compression, strongly differ from those of hydrocarbon systems in strike-slip
415 regimes, e.g. the Bohai Bay Basin (China). In the Bohai Bay Basin, the main source of fluids is the
416 mantle with minor thermal decomposition (Zhang et al., 2008). In that case, the fluids from the
417 mantle upraise along subvertical faults crossing the basement, which are lacking in the Apennines
418 (Picotti and Pazzaglia, 2008).

419 Despite our data do not permit to analyze the fluid-rock interaction, i.e. cementation vs.
420 hydrothermal processes, other studies based on core analyses have evidenced that cementation in
421 thrust systems is dominantly controlled by layer parallel shortening in the footwall of thrusts,
422 whereas hydrothermal processes are related to vertical migration of fluids within the thrust pile
423 (Roure et al., 2005). Based on (a) the sub-vertical distribution of the 2000 events, (b) the probable
424 thermal origin of the involved fluids (see previous section), and (c) the above considerations, we
425 suggest that the fluid-rock interaction at seismogenetic depth is mainly related to hydrothermal
426 processes.

427

428 **5. Conclusions**

429

430 The results of this study can be summarized in the following main points:

431 (a) The 2000 sequence developed along different, superimposed, WNW-ESE
432 striking thrusts, which are parallel to the Northern Apennine chain axis. This
433 feature contrasts to that observed in accretionary wedges, where the seismicity
434 generally develops along a single detachment surface (sole thrust).

435 (b) The stress field is consistent with that acting at a regional scale in the outer
436 sector of the chain.

(c) Fluids (oil and gas) play a role in the evolution of the sequence. These fluids are stored within the Cretaceous-Triassic limestones involved in the accretionary wedge of the chain, and upraise along sub-vertical fractures. These fractures activate in response to the compressive stress field responsible for the shortening of the wedge.

(d) The 2000 earthquakes, which develop in the outer sectors of Northern Apennines, involve methane-rich fluids upraising within the upper crust, whereas the events related to the extensional strain field affecting the inner sectors of the Apennine chain are mainly due to the uprising of CO_2 fluids from the mantle.

(e) The 2000 sequence occurred in an area that separates two distinct petroleum systems: a thermogenic and deeper system (to the northwest) involving carbonate reservoirs, and a shallower biogenic to mixed thermogenic-biogenic system (to the southeast) involving Neogene and Pliocene siliciclastic reservoirs. This bi-partition of the hydrocarbon systems controls the attenuation properties of the upper crust.

(f) The fluid-rock interaction at seismogenetic depth is driven by hydrothermal processes.

(g) The earthquakes in hydrocarbon-rich accretionary wedges may result from the complex interplay between tectonic stress and fluid pressure. The tectonic stress induces an overpressure in deep reservoirs and a fluid migration towards the shallower ones. The overpressure is related to tectonic compaction. The associated seismicity is characterized by (1) subvertical clouds of events, (2) diffusive-like time evolution, and (3) upward migration of the hypocenters.

Further studies on seismic sequences in Northern Apennines and other hydrocarbon-rich belts will allow us to (1) better constrain the kinematic picture exposed above, and (2) provide new insights on the role of fluids in controlling the seismicity in accretionary wedges.

Acknowledgements This study was supported by INGV-DPC funds. Thanks to François Roure for the perceptive review of the manuscript and to editor Claude Jaupart for the editorial handling. Thanks to all of the people who participated during the development of the temporary seismic network and took part in the phase-picking.

References

Alvarez, W., 1972. Rotation of the Corsica-Sardinia microplate. Nature Physical Science 235, 103 105.

Antonioli, A.; Piccinini, D.; Chiaraluce, L., Cocco M., 2005. Fluid flow and seismicity pattern: Evidence from the 1997 Umbria-Marche (central Italy) seismic sequence. Geophys. Res. Lett. 32(10), doi:10.1029/2004GL022256.

Audigane, P., Royer, J.J.,. Kaieda, H., 2002. Permeability characterization of the Soultz and Ogachi large-scale reservoir using induced microseismicity. Geophysics 67(1), 204– 211.

Bangs, N.L., Shipley, T.H., Moore, J.C., 1999. Fluid accumulation and channeling along the northern Barbados Ridge decollement thrust. J.Geophys Res. 104 (B9), 20399-20414.

Barchi, M.R., Minelli G., Pialli, G., 1998. The CROP 03 profile: a synthesis of results on deep structures of the northern Apennines. Mem. Soc. Geol. Ital. 52, 383-400.

Bartolini, C., Caputo R., Pieri, M., 1996. Pliocene-Quaternary sedimentation in the Northern Apennine Foredeep and related denudation. Geological Magazine 133, 3, 255-273.

Basili, R., Barba, S., 2007. Migration and shortening rates in the northern Apennines, Italy: implications for seismic hazard. Terra Nova 19, 462–468, doi: 10.1111/j.1365-3121.2007.00772.x.

Basili R., Valensise, G., Vannoli, P., Burrato, P. Fracassi, U., Mariano, S., Tiberti, M.M., Boschi, E., 2008. The Database of Individual Seismogenic Sources (DISS), version 3: summarizing 20 years of research on Italy's earthquake geology. Tectonophysics, doi:10.1016/j.tecto.2007.04.014.

Boccaletti, M., Bonini, M., Corti, G., Gasperini, P., Martelli, L., Piccardi, L., Severi P., Vannucci G., 2004. Carta sismotettonica della Regione Emilia-Romagna – Note Illustrative, in: Boccaletti, M., Martelli, L. (eds), S.EL.CA. (Firenze), pp. 60.

Boccaletti, M., Coli, M., Eva, C., Ferrari, G., Giglia, G., Lazzarotto, A., Merlanti, F., Nicolich, R., Papani, G., Postpischl D., 1985. Considerations on the seismotectonics of the Northern Apennines, Tectonophysics 117, 7-38.

496 Bonini, M., 2007. Interrelations of mud volcanism, fluid venting, and thrust-anticline folding:
497 Examples from the external northern Apennines (Emilia-Romagna, Italy). J. Geophys. Res. 112,
498 B08413. doi:10.1029/2006JB004859.
499 Boore, D.M., 1983. Stochastic simulation of high-frequency ground motions based on
500 seismological models of the radiated spectra. Bull. Seismol. Soc. Am. 73 (6A), 1865-1894.
501 Brown, K.M., Kopf, A., Underwood, M.B., Weinberger, J.L., 2003. Compositional and fluid
502 pressure controls on the state of stress on the Nankai subduction thrust: A weak plate boundary.
503 Earth Planet. Sci. Lett. 214, 589-603.
504 Brune, N., 1970. Tectonic stress and the spectra of seismic shear waves from earthquakes. J.
505 Geophys. Res. 75, 4997–5009.
506 Burrato P., Poli, M.E., Vannoli, P., Zanferrari, A., Basili, R., Galadini, F., 2008. Sources of Mw 5+
507 earthquakes in northeastern Italy and western Slovenia: an updated view based on geological and
508 seismological evidence. Tectonophysics, doi:10.1016/j.tecto.2007.07.009.
509 Burrato, P., Ciucci, F., Valensise, G., 2003. An inventory of river anomalies in the Po Plain,
510 Northern Italy: evidence for active blind thrust faulting. Annals of Geophysics 46, 5, 865-882.
511 Byerlee, J.D., 1978. Friction of rocks. Pure Appl. Geophys. 116, 615-626.
512 Capozzi R., Picotti, V., 2002. Fluid migration and origin of a mud volcano in the Northern
513 Apennines (Italy): the role of deeply rooted normal faults. Terra Nova 14, 5, 363–370.
514 Castello, B., Selvaggi, G., Chiarabba, C., Amato A., 2005. CSI Catalogo della sismicità italiana
515 1981-2002, versione 1.0. INGV-CNT, Roma.
516 Chiodini G., Cardellini, C., Amato, A., Boschi, E., Caliro, S., Frondini, F., Ventura G., 2004.
517 Carbon dioxide Earth degassing and seismogenesis in central and southern Italy. Geophys. Res.
518 Lett. 31, L07615. doi:10.1029/2004GL019480.
519 Ciaccio, M.G., Chiarabba C., 2002. Tomographic models and seismotectonics of the Reggio Emilia
520 region, Italy. Tectonophysics 344, 261–276.
521 Cochrane, G.R., Moore, J.C., MacKay, M.E., and Moore, G.F., 1994. Velocity and inferred porosity
522 model of the Oregon accretionary prism from multichannel seismic reflection data: implications
523 on sediment dewatering and overpressure. J. Geophys. Res. 99, 7033–7043.
524 CPTI Working Group CPTI (2004). Catalogo Parametrico dei Terremoti Italiani, vers. 2004
525 (CPT104), INGV Bologna, http://emidius.mi.ingv.it/CPTI.
526 CSTI 1.0 Working Group 2001. Catalogo strumentale dei terremoti italiani dal 1981 al 1996,
527 Version 1.0 ISBN 88-491-1734-5 Clueb Bologna, CD-ROM.
528 Di Giovambattista, R., Tyupkin Yu.S.,1999. The fine structure of the dynamics of seismicity before
529 M≥ 4.5 earthquakes in the area of Reggio Emilia (Northern Italy). Ann. Geof., 42, 897-909.

530 DISS Working Group, 2007. Database of Individual Seismogenic Sources (DISS), Version 3.0.4: A
531 compilation of potential sources for earthquakes larger than M 5.5 in Italy and surrounding areas,
532 http://www.ingv.it/DISS/, © INGV 2005, 2007.
533 Doglioni, C., 1991. A proposal of kinematic modeling for W-dipping subductions. Possible
534 applications to the Tyrrhenian Apennines system. Terra Nova 3, 423-434.
535 Doglioni, C., 1993. Some remarks of the origin of foredeeps. Tectonophysics 228, 1-20.
536 Eberhart-Phillips, D., Michael, A.J., 1993. Three dimensional velocity structure, seismicity, and
537 fault structure in the Parkfield region, central California. J. Geophys Res. 98, 15737–15758.
538 Etiope G., Martinelli, G., Caracausi, A., Italiano, F., 2007. Methane seeps and mud volcanoes in
539 Italy: Gas origin, fractionation and emission to the atmosphere. Gephys. Res. Lett. 34, L14303.
540 doi:10.1029/2007GL030341.
541 Flanagan, M.P., Wiens, D.A., 1994. Radial upper mantle attenuation structure of inactive back-arc
542 basins from differential shear wave measurements. J. Geophys. Res. 99, 15469-15485.
543 Fournier, R., 1996. Compressive and tensile failure at high fluid pressure where preexisting
544 fractures have cohesive strength, with application to the San Andreas Fault. J. Geophys. Res.
545 101(B11), 25499-25509.
546 Gephart, J.W., Forsyth D.W., 1984. An improved method for determining the regional stress tensor
547 using earthquake focal mechanism data: Application to the San Fernando earthquake sequenze.
548 J. Geophys. Res. 89, 9305–9320.
549 Gratier J.P., Favreau P., Renard F., Pili E., 2002, Fluid pressure evolution during the earthquake
550 cycle controlled by fluid flow and pressure solution crack sealing. Earth Planets and Space,54,
551 1139-1146.
552 Husen, S., Kissling, E., 2001. Postseismic fluid flow after the large subduction earthquake of
553 Antofagasta, Chile. Geology 29, 847–850.
554 Karig D, Ingle JC, Bouma AH Ellis H, Haulen N, Koizumi I, MacGreor ID, Moore C, UJiee H,
555 Watanabe T, White SM, Yasui M, Ling HY, 1973. Origin of west Phipinne Basin. Nature, 246,
556 458-461.
557 Kissling, E., Kradolfer, U., Maurer H., 1995. VELEST user's guide:short introduction, Technical
558 Rept., Institute of Geophysics and Swiss Seismological Service, ETH-Zürich.
559 Kondo, H., Kimura, G., Masago, H., Ohmori-Ikehara, K., Kitamura, Y., Ikesawa, E., Sakaguchi, A.,
560 Yamaguchi, A., Okamoto S., 2005. Deformation and fluid flow of a major out-of-sequence thrust
561 located at seismogenic depth in an accretionary complex: Nobeoka Thrust in the Shimanto Belt,
562 Kyushu, Japan. Tectonics 24, TC6008. doi:10.1029/2004TC001655.
563 Labaume P., Sheppard S.M.F., Moretti I., 2001. Fluid flow in cataclastic thrust fault zones in
564 sandstones, Sub-Andean Zone, southern Bolivia. Tectonophysics 340, 141-172.

565 Lahr, J.C., 1999. HYPOELLIPSE Y2K: A Computer Program for Determining Local Earthquake
566 Hypocentral Parameters, Magnitude, and First-motion Pattern, U.S. Geological Survey Open-
567 fileReport 99-023, paper (112 pp.) and online (http://greenwood.cr.usgs.gov/pub/open-file-
568 reports/ofr-99-0023).
569 Lavecchia, G., Boncio P., Creati N., 2003. A lithosperic-scale seismogenic thrust in central Italy. J.
570 Geodyn. 36, 79-94.
571 Lindquist, S.J., 1999. Petroleum Systems of the Po Basin Province of Northern Italy and the
572 Northern Adriatic Sea: Porto Garibaldi (Biogenic), Meride/Riva di Solto (Thermal), and
573 Marnoso Arenacea (Thermal). USGS Open-File Report 99-50-M.
574 Malagnini, L., Hermann R.B., Di Bona M., 2000. Ground-motion scaling in the Apennines (Italy).
575 Bull. Seismol. Soc. Am. 90 (4), 1062-1081.
576 Malin, P., Shalev E., Balven H., Lewis-Kenedi C., 2006. Structure of the San Andreas Fault at
577 SAFOD from P-wave tomography and fault-guided wave mapping, Geophys. Res. Lett., 33,
578 L13314, doi:10.1029/2006GL025973.
579 Mariucci, M.T., Müller B., 2003. The tectonic regime in Italy inferred from borehole breakout data.
580 Tectonophysics 361, 21-35.
581 Martinelli, G., Judd, A., 2004. Mud volcanoes of Italy. Geol. J. 39, 49– 61.
582 Massoli, D., Koyi, H.A., Barchi, M.R., 2006. Structural evolution of a fold and thrust belt generated
583 by multiple décollements: analogue models and natural examples from the Northern Apennines
584 (Italy). Journal of Structural Geology 28, 185-199.
585 Miller S.A., 1996. Fluid-mediated influence of adjacent thrusting on the seismic cycle at Parkfield.
586 Nature 382, 799 – 802.
587 Muco, B., 1998. Twenty years seismic monitoring of induced seismicity in northern Albania. Pure
588 Appl. Geophys. 153, 151–162.
589 Montone, P., Mariucci, M.T., Pondrelli, S., Amato, A., 2004. An improved stress map for Italy and
590 surrounding regions (central Mediterranean). J. Geophys. Res. 109, doi: 10.1029/2003JB002703,
591 2004.
592 Mourgues, R, Cobbold, P.R., 2006. Thrust wedges and fluid overpressures: Sandbox models
593 involving pore fluids. J. Geophys. Res. B05404. doi:10.1029/2004JB003441.
594 Moretti, I. , Delhomme J. P., Cornet F., Bernard P., Schmidt-Hattenberger C. and Borm G., 2002.
595 The Corinth Rift Laboratory: monitoring of active faults. First break volume 20.2 February 2002.
596 Orlov, A., V. Omelchenko, A. Trubenko, and F. Schneider, 2004. Incidence of tectonic stress on
597 overpressure development in Ukrainian basins. In Swennen R., Roure F., and Granath J. W.,
598 eds., Deformation, fluid flow, and reservoir appraisal in foreland fold and thrust belts: AAPG
599 Hedberg Series, no. 1, 245–255.

600 Perez, R.J., Boles, J.R., 2004. Mineralization, fluid flow, and sealing properties associated with an
601 active thrust fault: San Joaquin basin, California. AAPG Bullettin 88, 1295-1314.
602 Piccinini, D., Chiarabba, C., Augliera, P., Monghidoro Earthquake Group (M.E.G.), 2006.
603 Compression along the northern Apennines? Evidence from the Mw 5.3 Monghidoro earthquake.
604 Terra Nova 18 (2) , 89–94. doi:10.1111/j.1365-3121.2005.00667.
605 Picotti, V., Capozzi, G., Bertozzi, G., Mosca, F., Sitta, A., Tornaghi, M., 2007. The Miocene
606 Petroleum System of the Northern Apennines in the Central Po Plain (Italy). In: Lacombe, O.;
607 Lavé, J.; Roure, F.; Verges, J. eds., Thrust Belts and Foreland Basins, Springer Verlag, Berlin,
608 117-131.
609 Picotti, V., Pazzaglia F. J. , 2008. A new active tectonic model for the construction of the Northern
610 Apennines mountain front near Bologna (Italy). J. Geophys. Res., 113, B08412,
611 doi:10.1029/2007JB005307.
612 Pieri, M., Groppi G., 1981. Subsurface geological structure of the Po Plain (Italy). Pubbl. P.F.G.-
613 C.N.R., 414, 1-23.
614 Pondrelli, S., Salimbeni, S., Ekström, G., Morelli, A., Gasperini P., Vannucci, G., 2006. The Italian
615 CMT dataset from 1977 to the present. Phys. Earth.Planet.Int.
616 doi:10.1016/j.pepi.2006.07.008,159/3-4.
617 Reasenberg, P., Oppenheimer D., 1985. FPFIT, FPPLOT and FPPAGE: fortran computer programs
618 for calculating and displaying earthquake fault plane solutions. U.S.G.S., Open File Rep., 85-
619 739.
620 RER, ENI-Agip, 1998. Riserve idriche sotterranee della Regione Emilia Romagna. Di Dio, G. (Ed),
621 S.EL.CA. (Firenze), 120 pp..
622 Roure, F., Swennen, R., Schneider, F.J., Faure, L., Ferket, H., Guilhaumou, N., Osadetz, K.,
623 Robion, P., Vandeginste, V., 2005. Incidence and importance of tectonics and natural fluid
624 migration on reservoir evolution in foreland fold-and-thrust belts. Oil & Gas Science and
625 Technology - Rev. IFP, 60(1), 67-106. doi: 10.2516/ogst:2005006.
626 Schneider, F., 2003. Basin modelling in complex area: Examples from Eastern Venezuelan and
627 Canadian foothills. Oil & Gas Science and Technology – Rev. IFP, 58, 2, 313-324.
628 Scrocca, D., Carminati, E., Doglioni, C., Marcantoni, D., 2007. Slab retreat and active shortening
629 along the central-northern Apennines, in: Lacombe, O., Lavé, J., Roure, F., Verges, J. (Eds.),
630 Thrust belts and Foreland Basins: from fold kinematics to hydrocarbon systems. Frontiers in
631 Earth Sciences, Springer, 471-487.
632 Shapiro, S.A., Patzig, R., Rothert, E., Rindschwentner J., 2003. Triggering of seismicity by pore
633 pressure perturbations: Permeability related signatures of the phenomenon. Pure Appl. Geophys.
634 160, 1051–1066.

635 Shapiro, S.A., Huenges, E., Borm G., 1997. Estimating the crust permeability from fluid-injection-
636 induced seismic emission at the KTB site. Geophys. J. Int. 131, F15–F18.
637 Sibson, RH., 2005. Hinge-parallel fluid flow in fold-thrust belts: how widespread?. Proocedings of
638 The Geologists Association 116, 301-309.
639 Sibson, R.H., 2000. Fluid involvement in normal faulting. J. Geodyn. 29, 469-499.
640 Talwani, P., Chen, L., Gahalaut K., 2007. Seismogenic permeability, k_s. J. Geophys. Res. 112,
641 B07309. doi:10.1029/2006JB004665.
642 Tompkins, M., Christensen N., 1999. Effects of Pore Pressure on Compressional Wave Attenuation
643 in a Young Oceanic Basalt. Geophys. Res. Lett. 26 (9), 1321-1324.
644 Vannoli, P., Basili, R., Valensise, G., 2004. New geomorphic evidence for anticlinal growth driven
645 by blind-thrust faulting along the northern Marche coastal belt (central Italy). J. Seismol. 8, 297–
646 312.
647 Ventura, G., Vilardo G., 1999. Seismic-Based Estimate of Hydraulic Parameters at Vesuvius
648 Volcano. Geophys. Res. Lett. 26 (7), 887–890.
649 Winkler, K.W., Nur A., 1982. Seismic attenuation: effects of pore fluids and frictional sliding.
650 Geophys. 47, 1–15.
651 Yonkee W.A., Parry W.T., Bruhn R.L., 2003. Relations between progressive deformation and fluid-
652 rock interaction during shear-zone growth in a basement-cored thrust sheet, Sevier orogenic belt,
653 Utah. American Journal of Science 303, 1-59.
654 Zhang, T., Zhang, M., Bai, B., Wang, X., Li, L., 2008.Origin and accumulation of carbon dioxide in
655 the Huanghua depression, Bohai Bay Basin, China AAPG Bulletin 92, 341-358.
656 Zhao, D., Negishi, H., 1998. The 1995 Kobe earthquake: Seismic image of the source zone and its
657 implications for the rupture nucleation. J. Geophys Res. 103, 9967–9986.
658
659
660
661
662
663
664
665
666
667
668
669
670
671
672
673
674
675

676 **Figure captions**

677 **Figure 1.** (a) Seismotectonic sketch of the study area showing: historical seismicity of Mw ≥
678 5.5, red squares (CPTI Working Group, 2004); epicenters of the Faenza 2000 seismic sequences,
679 red circles (this study); epicenters of the Monghidoro 2003 seismic sequences, white stars (Piccinini
680 et al., 2006); focal mechanisms of the strongest events of the two sequences (from Pondrelli et al.,
681 2006); surface projection of individual seismogenic sources, orange rectangles (DISS Working
682 Group, 2007; http://www.ingv.it/DISS/); trace of the main Northern Apennines thrust fronts;
683 temporary stations used in this study, blue triangles; mud volcanoes and CH_4 seeps, yellow and
684 orange triangles, respectively (from Martinelli and Judd, 2004) and the isobathes of the base of the
685 Pliocene, yellow dashed lines. Localities: Bologna, BO; Faenza, FA; Forlì, FO; Ravenna, RA. Inset:
686 location map of the study area in the framework of the Northern Apennines (NA) and Southern
687 Alps (SA) thrust fronts. The Northern Apennine oil provinces are also reported according to Etiope
688 et al. (2007). Individual seismogenic sources from DISS are shown as black rectangles. White and
689 black arrows highlight areas in extension along the Northern Apennines crest, and areas in
690 compression along the Po Plain margins, respectively. Structures: Monferrato folds, Mf; Emilia
691 folds, Ef; Ferrara-Romagna folds, Ff; Pede-appenninic Thrust Front, PTF. The map uses the 90 m
692 SRTM DEM as topographic base (http://srtm.csi.cgiar.org). (b) Cross-section showing hypocenters
693 of the Faenza 2000 earthquakes plotted onto schematic geology (data from Boccaletti et al., 2004
694 and Massoli et al., 2006). The individual seismogenic sources of the 1781 (A) and 1688 (B)
695 earthquakes are shown as thick orange lines. Trace of the section is in (a). (c) Lithostratigraphic
696 scheme showing position of the main hydrocarbon reservoirs and seal rocks in the sedimentary
697 sequence, and occurrence of fresh waters and brine fluids (modified from Lindquist, 1999).

698 **Figure 2.** Seismogram of a microearthquake recorded by two stations of the mobile network
699 located in the two different attenuative zone across the source region. The station code is at top left.
700 The seismograms show a strong waveform variability in the two stations. Black lines point out
701 observed P, Ps,and S first-arrival times.

Figure 3. (a) Starting (dashed line) and final 1-D velocity model obtained using the Velest code. (b) Wadati diagram obtained using 5852 arrivals. Fitting DTs vs. DTp for all the available pairs of stations gives the value of the slope V_P/V_S=2.324±0.08. The linear correlation coefficient R is 0.96.

Figure 4. (a) Epicentral distribution of the re-located earthquakes as a function of time. (b) Hypocentral distribution of the re-located events as a function of time along a NNW-SSE section. (c) Hypocentral distribution of the re-located events as a function of time along a NE-SW section.

Figure 5. Spectral ratios of the earthquakes with magnitude grater than 3.0 versus CAST reference station (location in Fig. 1). The thicker, horizontal line represents the constant value of the ratio. We show the stations characterized by a low attenuation value (left panel) and higher value (right panel).

Figure 6. The observed displacement spectrum for events with magnitude larger than 4 corrected with equation 1 is matched by the theoretical curves corresponding to ω^2 spectrum with a constant stress drop of 100 bar. $Q_{S,Staz}$ are reported in the Table 2. $Q_{S,CAST}$.

Figure 7. (a) Focal mechanisms of earthquakes (size proportional to the magnitude of the events) and distribution of P and T axes (Schmidt net, lower hemisphere). (b) Strike, dip and rake of nodal planes of focal mechansims. The histograms are also reported. (c) Results of the stress field analysis of focal mechanisms.

Figure 8. *r-t* plot of the Faenza 2000 relocated events. All the events lie below the parabolic envelope for D = 1.9 m^2/s. The spatio-temporal seismicity pattern shows vertically clustered events interrupted by time intervals of seismic quiescence.

Table 1. Estimate of the Qs values using the spectral-ratios method shown in Fig. 5.

Station	$Q_{S,Cast} = \infty$ $Q_{S,STAZ}$	$Q_{S,Cast} = 500$ $Q_{S,STAZ}$	$Q_{S,Cast} = 250$ $Q_{S,STAZ}$	$Q_{S,Cast} = 100$ $Q_{S,STAZ}$
CESA	128	103	87	58
COLL	-	510	334	175
FILE	190	146	119	76
PETE	-	-	403	140
SGIO	457	342	209	101
SGIO	174	124	94	58
TULL	220	155	117	67

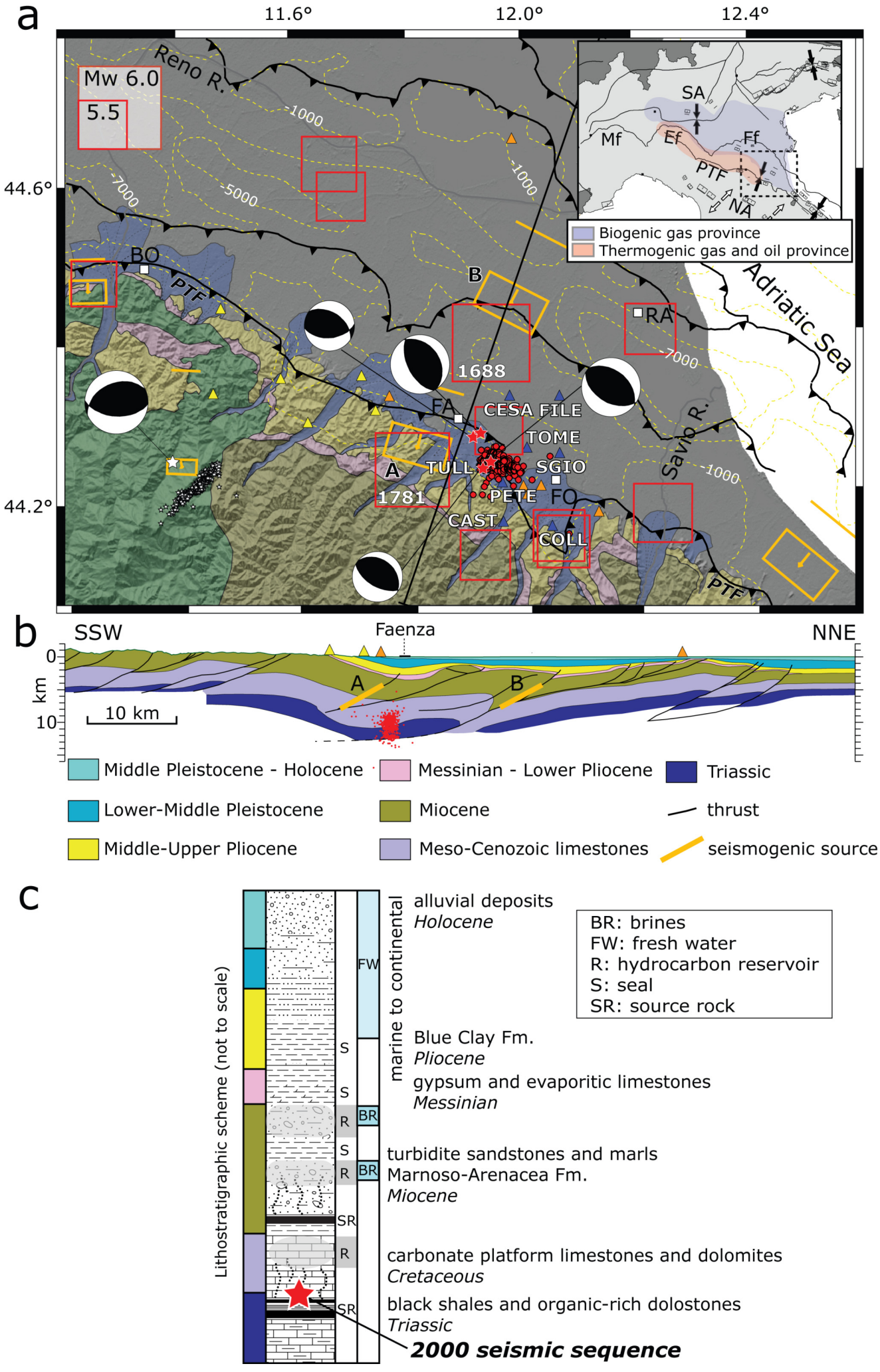
a
11.6°
12.0°
12.4°
44.6°
44.2°
Reno R.
Mw 6.0
5.5
-1000
-7000
-5000
BO
PTF
B
1688
RA
Adriatic Sea
FA
CESA FILE
TOME
A
TULL
SGIO
1781
PETE
FO
CAST
COLL
Savio R.
SA
Mf
Ef
Ff
NA
Biogenic gas province
Thermogenic gas and oil province
b
SSW
Faenza
NNE
km
0
10
10 km
Middle Pleistocene - Holocene
Messinian - Lower Pliocene
Triassic
Lower-Middle Pleistocene
Miocene
thrust
Middle-Upper Pliocene
Meso-Cenozoic limestones
seismogenic source
c
Lithostratigraphic scheme (not to scale)
marine to continental
FW
S
S
R
BR
S
R
BR
SR
R
SR
alluvial deposits
Holocene
BR: brines
FW: fresh water
R: hydrocarbon reservoir
S: seal
SR: source rock
Blue Clay Fm.
Pliocene
gypsum and evaporitic limestones
Messinian
turbidite sandstones and marls
Marnoso-Arenacea Fm.
Miocene
carbonate platform limestones and dolomites
Cretaceous
black shales and organic-rich dolostones
Triassic
2000 seismic sequence

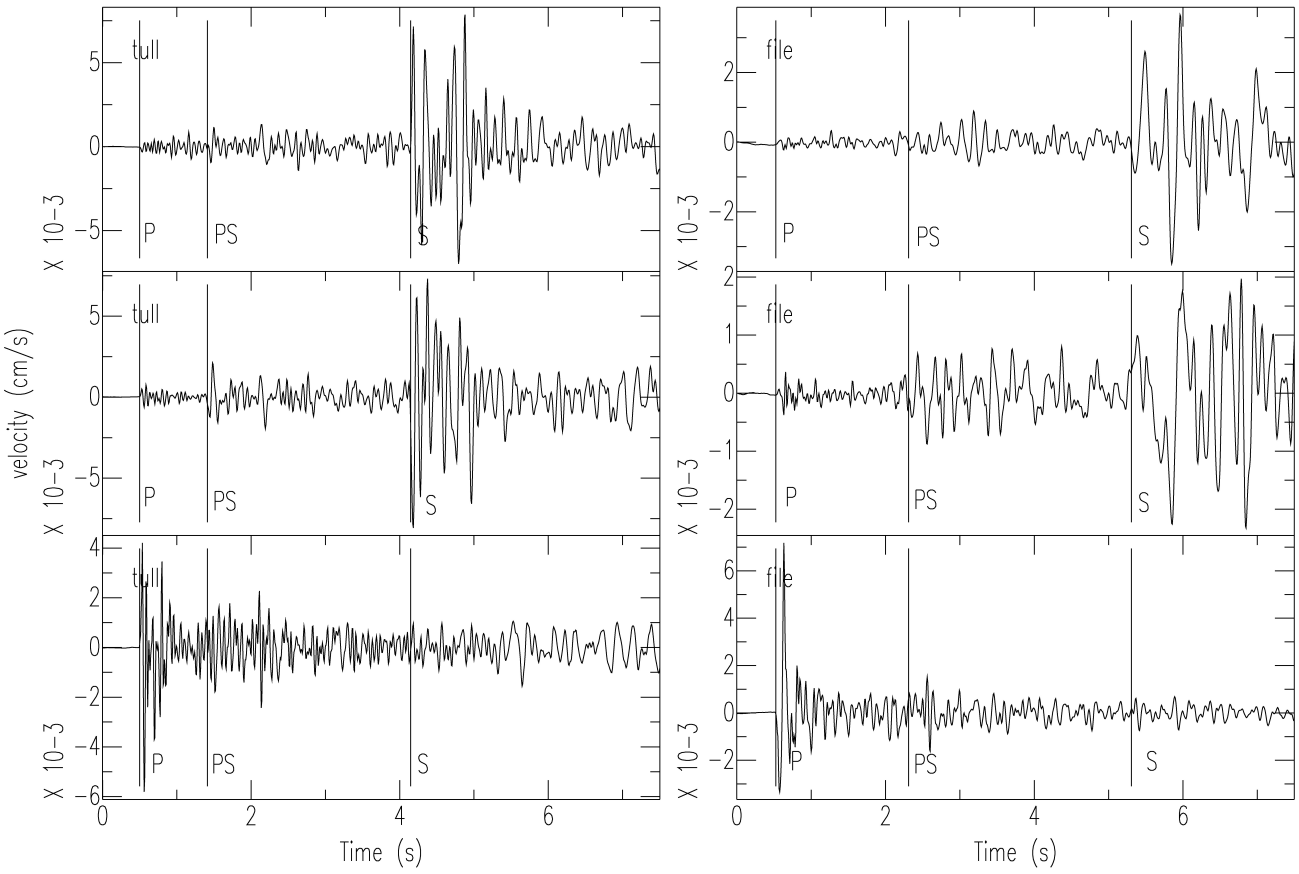
velocity (cm/s)
tull
file
P
PS
S
X 10−3
Time (s)

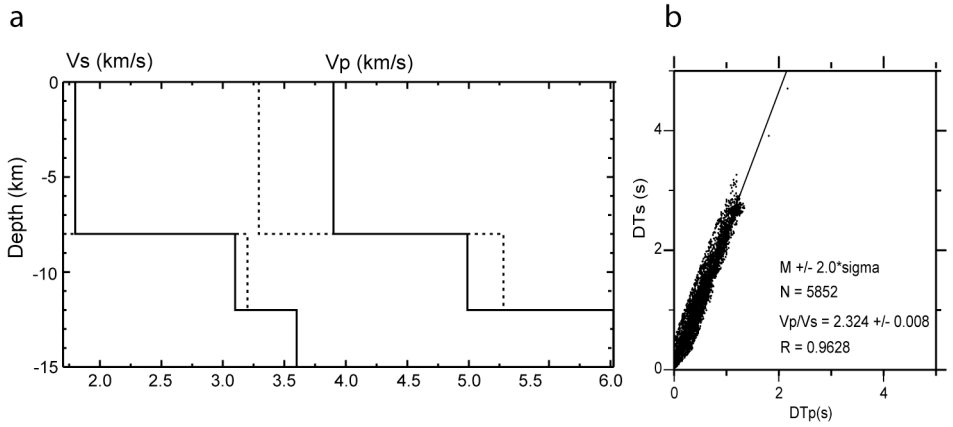
a
Vs (km/s)
Vp (km/s)
Depth (km)
0
-5
-10
-15
2.0
2.5
3.0
3.5
4.0
4.5
5.0
5.5
6.0
b
DTs (s)
DTp(s)
0
2
4
M +/- 2.0*sigma
N = 5852
Vp/Vs = 2.324 +/- 0.008
R = 0.9628

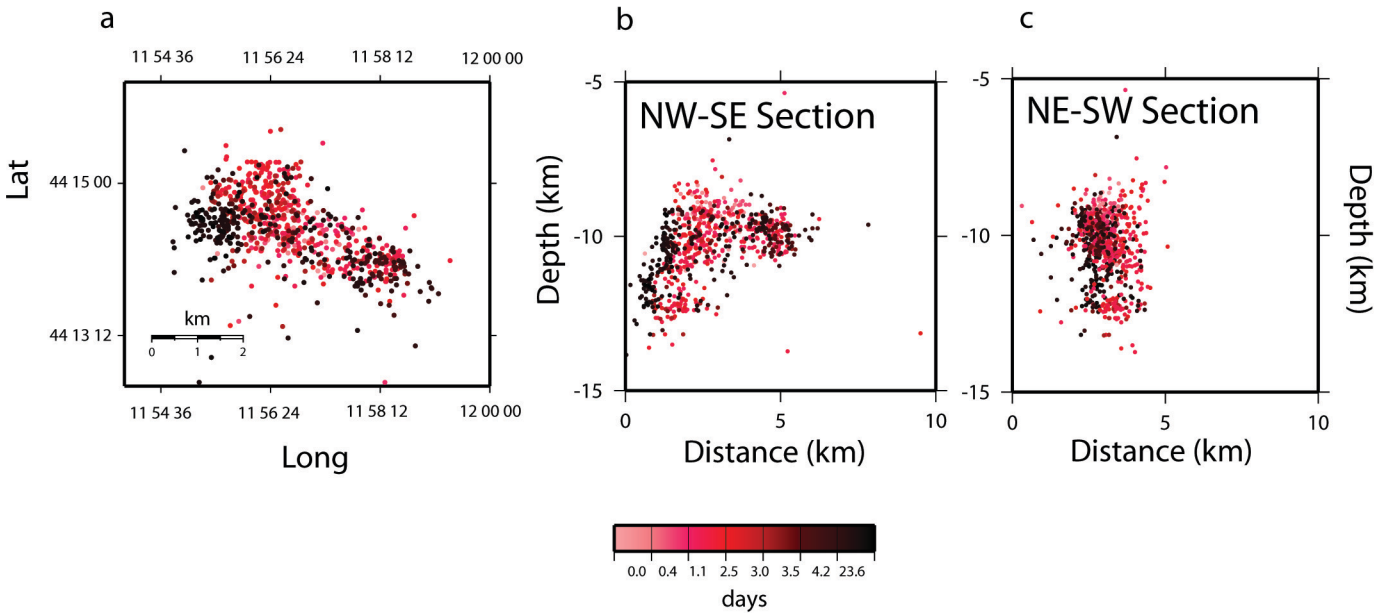
a
b
c
11 54 36
11 56 24
11 58 12
12 00 00
Lat
44 15 00
44 13 12
km
0
1
2
Long
Depth (km)
-5
-10
-15
NW-SE Section
0
5
10
Distance (km)
NE-SW Section
0.0 0.4 1.1 2.5 3.0 3.5 4.2 23.6
days

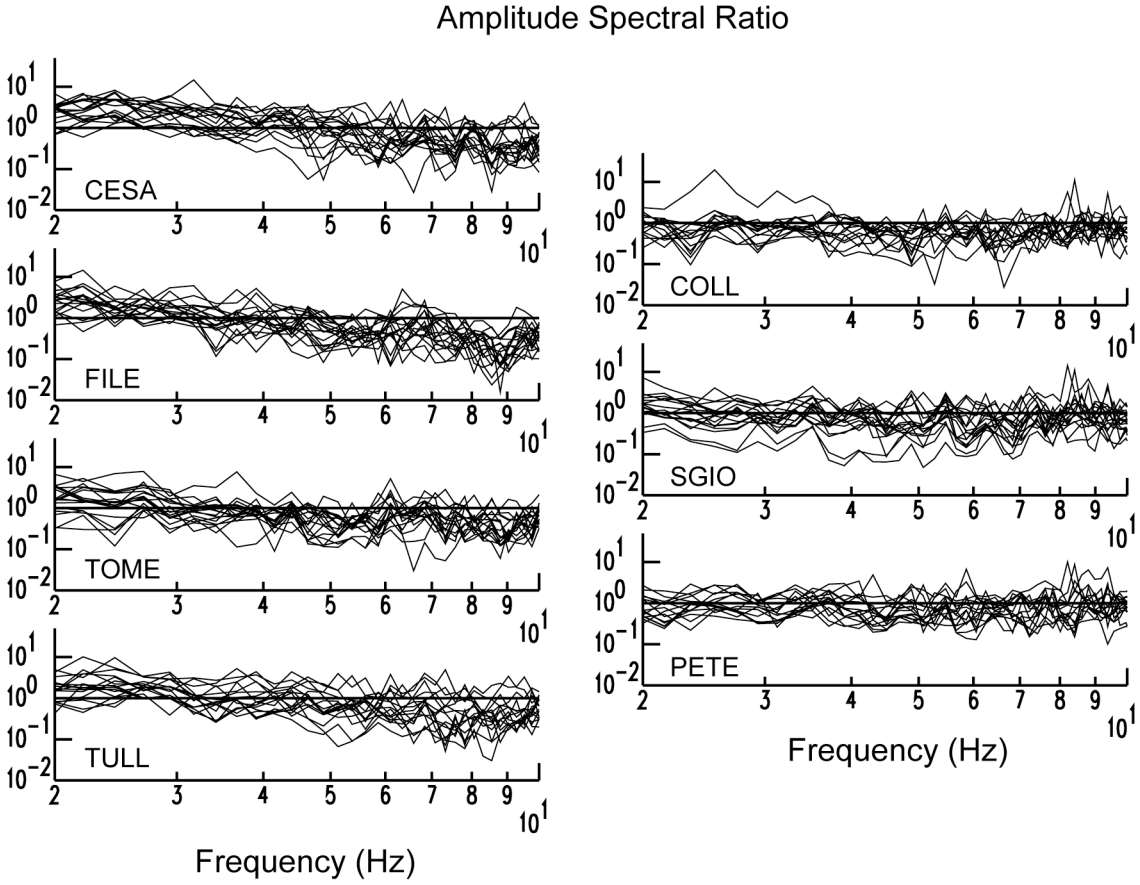
Amplitude Spectral Ratio
CESA
FILE
TOME
TULL
COLL
SGIO
PETE
Frequency (Hz)
Frequency (Hz)

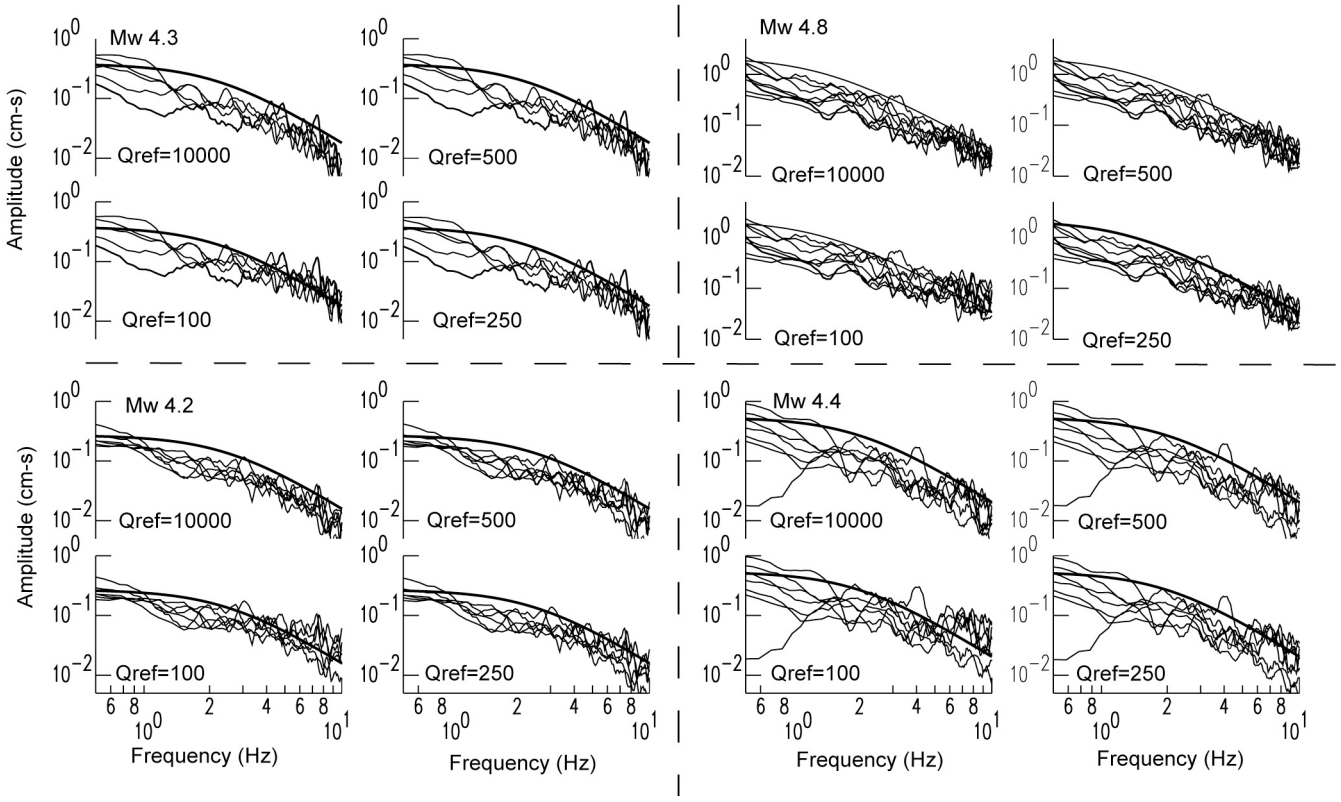
Mw 4.3
Mw 4.8
Mw 4.2
Mw 4.4
Qref=10000
Qref=500
Qref=100
Qref=250
Amplitude (cm-s)
Frequency (Hz)

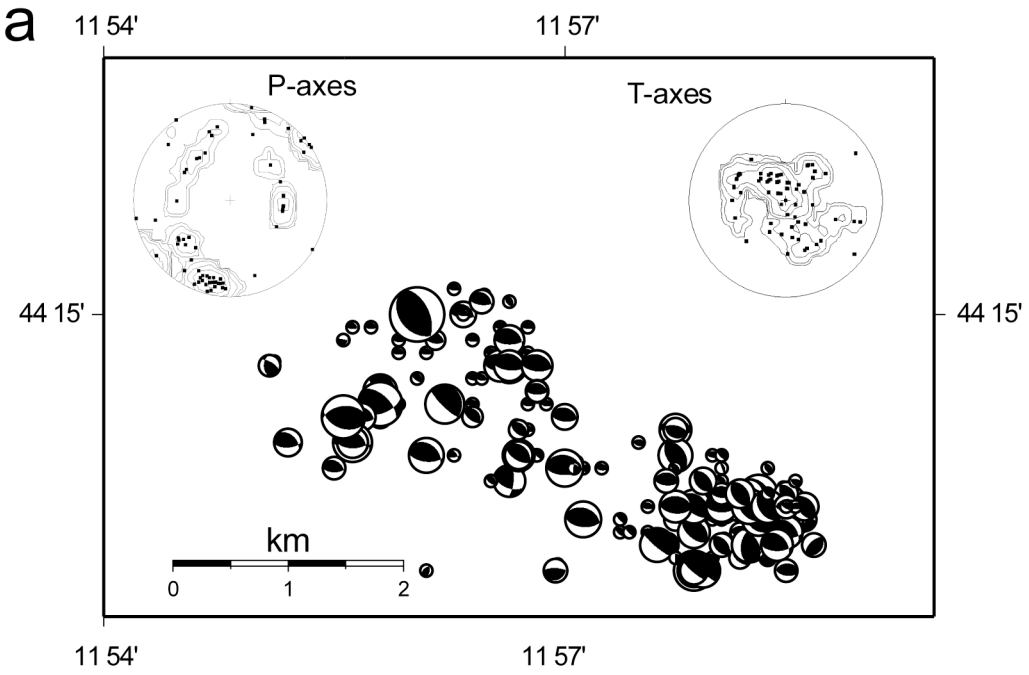
a
11 54'
11 57'
P-axes
T-axes
44 15'
44 15'
km
0
1
2
11 54'
11 57'

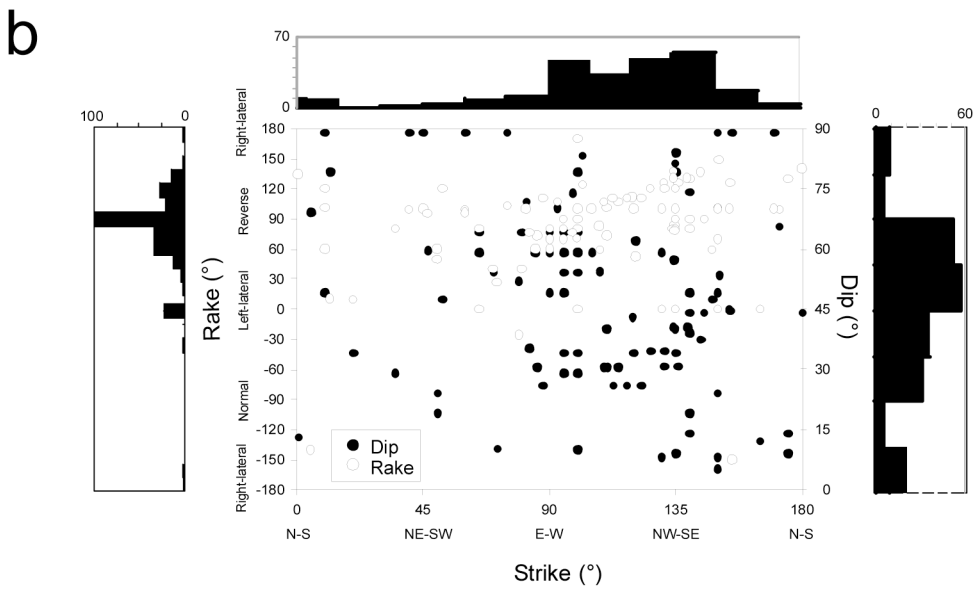
b
70
0
100
0
Right-lateral
Reverse
Left-lateral
Normal
Right-lateral
180
150
120
90
60
30
0
-30
-60
-90
-120
-150
-180
Rake (°)
90
75
60
45
30
15
0
Dip (°)
0
60
Dip
Rake
0
45
90
135
180
N-S
NE-SW
E-W
NW-SE
N-S
Strike (°)

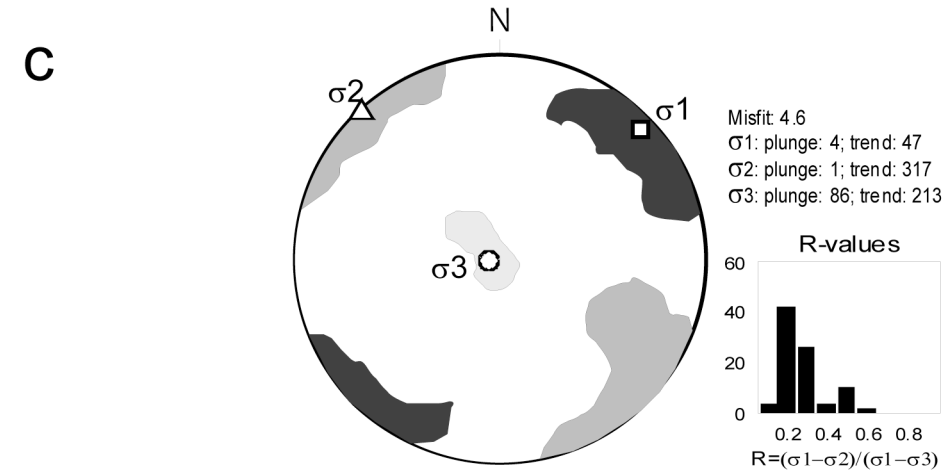
c
N
σ2
σ1
σ3
Misfit: 4.6
σ1: plunge: 4; trend: 47
σ2: plunge: 1; trend: 317
σ3: plunge: 86; trend: 213
R-values
60
40
20
0
0.2
0.4
0.6
0.8
R=(σ1−σ2)/(σ1−σ3)

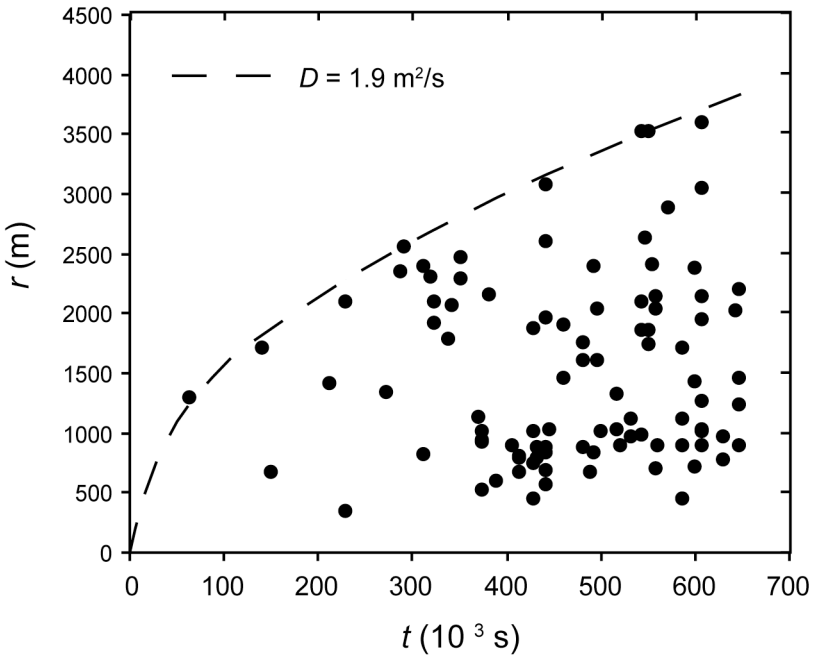
D = 1.9 m²/s
r (m)
t (10 ³ s)
0
500
1000
1500
2000
2500
3000
3500
4000
4500
0
100
200
300
400
500
600
700